doi: 10.32131/jes.6.35

Journal of the Earth Simulator, Volume 6, October 2006, 35–49

An Eddy-Resolving Simulation of the Quasi-Global Ocean Driven by Satellite-Observed Wind Field

– Preliminary Outcomes from Physical and Biological Fields –

Hideharu Sasaki[1]*, Yoshikazu Sasai[2], Masami Nonaka[2],
Yukio Masumoto[2, 3] and Shintaro Kawahara[1]

[1] *The Earth Simulator Center, Japan Agency for Marine-Earth Science and Technology (JAMSTEC), 3173-25 Showa-machi, Kanazawa-ku, Yokohama, Kanagawa, 236-0001 Japan*
[2] *Frontier Research Center for Global Change, Japan Agency for Marine-Earth Science and Technology (JAMSTEC), 3173-25 Showa-machi, Kanazawa-ku, Yokohama, Kanagawa, 236-0001 Japan*
[3] *Graduate School of Science, University of Tokyo, 7-3-1, Hongo, Bunkyo-ku, Tokyo, 113-0033, Japan*

(Received June 23, 2006; Revised manuscript accepted August 18, 2006)

Abstract An eddy-resolving quasi-global ocean simulation with marine ecosystem model driven by the QuikSCAT satellite wind field (QSCAT run) has been performed on the Earth Simulator to study responses of ocean circulations and marine biological fields to small scale structures in wind field by comparing with the simulation driven by the NCEP/NCAR reanalysis (NCEP run). In the QuikSCAT wind field, small structures related to orographic effects, air-sea interactions, and coastlines are observed, but these are not represented well in the reanalysis. The simulated oceanic fields driven by the satellite wind capture small scale responses of the ocean to the small scale structures in the wind field, which are not represented in the NCEP run. For example, small scale structures in the sea surface height variabilities are found in the equatorial oceans, the eastern tropical Pacific, and the western subtropical Pacific. In addition to these, some of the oceanic responses have large zonal extents with small meridional scales in the QSCAT run, for example, the Hawaiian Lee Countercurrent to the west of the Hawaiian Islands and two branches of south equatorial currents in the eastern equatorial Pacific. Biological fields in near-shore regions, for example along the California coast, are also simulated well in the QSCAT run due to realistic representation of coastal upwelling influenced by the near-shore wind field. These improvements in the QSCAT run suggest that realistic satellite wind field with small scale structures is necessary to represent small scale oceanic phenomena and biological fields appropriately in high-resolution ocean simulations.

Keywords: high-resolution ocean general circulation model, satellite-observed wind field, oceanic surface and subsurface fields, marine ecosystem

1. Introduction

Rapid development of computer system and ocean general circulation model (OGCM) with advanced parameterizations enable us to perform high-resolution global ocean simulation that represent well not only global circulation but also pathways of narrow strong western boundary currents and small scale phenomena including meso-scale eddies. Successful outcomes are reported in some projects: Global POP (Parallel Ocean Program) [1], Global OCCAM (Ocean Circulation and Advanced Modelling Project) [2], and the OFES (Ocean general circulation model for the Earth Simulator) [3, 4] projects. In the OFES project, we have performed a series of eddy-resolving simulations of the quasi-global ocean with horizontal resolution of 0.1° forced by NCEP/NCAR reanalysis data [5]. The horizontal resolution of the atmospheric reanalysis data that drive the simulation is about 2°.

Observational satellite systems, however, have been continuously providing us global ocean surface data with high spatial resolution in recent years. The QuikSCAT (QSCAT) satellite with a radar scatterometer called SeaWinds [6], which was launched in June 1999, has been observing surface wind fields at 25 km resolution over 90% of the global ocean daily. The observation has

* ***Corresponding author***: *Hideharu Sasaki, The Earth Simulator Center, Japan Agency for Marine-Earth Science and Technology (JAMSTEC), 3173-25 Showa-machi, Kanazawa-ku, Yokohama, Kanagawa, 236-0001 Japan. E-mail: sasaki@jamstec.go.jp*

been making some new findings not only in the surface wind field but also air-sea interaction in combination with satellite observed sea surface temperature (SST), cloud water, and ocean color. Xie et al. [7], for example, report that the QSCAT satellite captures a wake of weak winds behind each of the major Hawaiian Islands, and reveal air-sea interactions along the Hawaiian Lee Countercurrent (HLCC) triggered by wind curls in the lee of the islands. Chelton et al. [8] find the coupling between surface wind and SST accompanied by tropical instability waves in the eastern equatorial Pacific. Furthermore, Xie et al. [9] show air-sea interactions including chlorophyll activity in the eastern Pacific under the jets over the Central America.

In Figure 1, we compare the distribution of surface wind stress observed by the QSCAT satellite with that in the NCEP/NCAR reanalysis. Although overall features in the curl of the QSCAT wind stress are similar to those of the reanalysis wind stress, some discrepancies are also found between them, especially in the small scale orographic lee winds. As pointed out in the previous studies, there are small distinct structures of positive and negative curls in the satellite observation compared with those in the reanalysis, e.g., in the eastern Pacific and in the west of the Hawaiian Islands. In the equatorial oceans zonally elongated structures of positive and negative curls are found in the satellite observation, especially in the equatorial Pacific, but obscure in the reanalysis data (see also Figure 6). These structures might be related to air-sea interactions accompanied by equatorial currents [8]. Along some coastlines, relatively strong positive or negative curls are distributed in the reanalysis, for example,

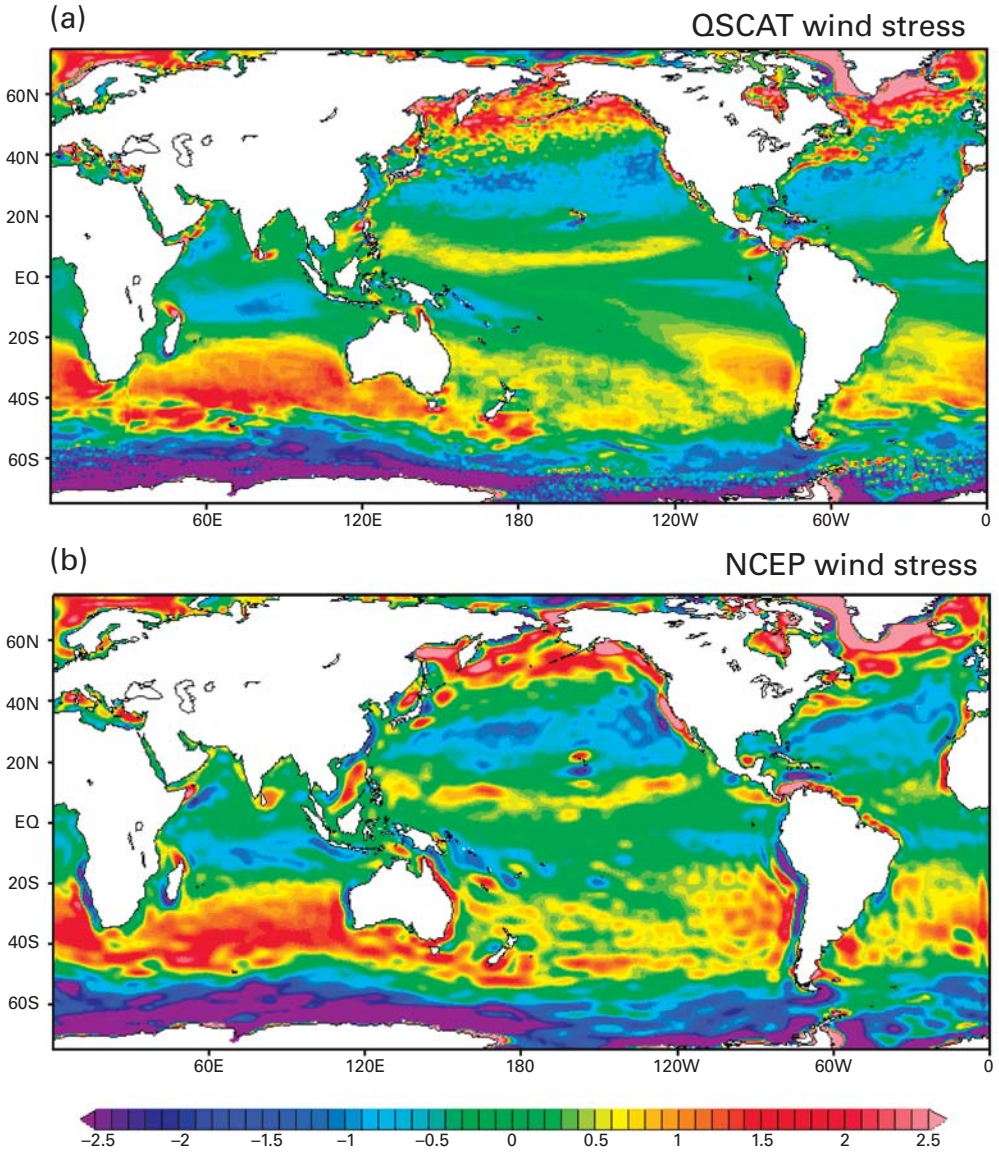

Fig. 1 Distributions of mean surface wind stress curl in common logarithm scale (10^{-7} N m^{-3}) averaged from 2001 to 2004 based on (a) the QSCAT satellite observation and (b) the NCEP/NCAR reanalysis.

there is negative curl along the west coast of the South America. In the South China and Japan Seas and to the south and east of Japan, relatively broad positive curls are found in the reanalysis compared to those with small structures in the satellite observation. These discrepancies imply that in the reanalysis system there are some difficulties to represent surface wind fields with small structures related to orographic effects, air-sea interactions, and coastlines realistically. Then, how the ocean responds to these wind structures that cannot be captured well in the reanalysis? This has not been understood enough. As the discrepancies in the wind fields tend to have small horizontal scales, oceanic responses can also have small scales. Thus, for its investigation, we need to conduct the simulations with high horizontal resolutions enough to resolve the expected oceanic responses.

Oceanic responses to small scale structures of winds can be important to marine biology, because the surface marine biology is influenced by the physical processes with global to frontal scales. The basin-wide scale simulation of ecosystem in the North Atlantic is performed by Oschlies and Garçon [10] using a simple four component nitrate-phytoplankton-zooplankton-detritus (NPZD) ecosystem model coupled with an eddy-permitting (1/3°) resolution model. In comparison with the eddy-permitting model, eddy-resolving (1/9°) models improve the simulated physical environments and clearly reproduce the aspect of seasonal cycle of surface chlorophyll, especially the spatial pattern in mid- and high-latitudes and in coastal upwelling regions [11, 12]. Sasai et al. [13] have performed a global scale simulation of marine ecosystem using the NPZD model embedded in an eddy-resolving OGCM forced by the NCEP/NCAR reanalysis. They show a realistic pattern of surface chlorophyll influenced by the western boundary current and the meso-scale phenomena such as eddies and frontal structures in the North Pacific. However, ocean models that are driven by coarse resolution atmospheric reanalysis products or climatological data tend to have difficulty in simulating the accurate coastal upwelling and currents in the eastern boundary regions [14]. Using a high-resolution wind fields observed by the QSCAT satellite, ocean model may improve the current system in near-shore regions and biological fields.

In this study, we investigate responses of ocean circulations and marine biological fields to small scale structures in wind field by comparing OGCM simulations driven by the wind stress fields of the QSCAT satellite observation and the NCEP/NCAR reanalysis. The paper is structured as follows. The OGCM and marine ecosystem model used in this study is described in Section 2. The physical and biological fields of the simulated results are shown in Section 3 and 4, respectively. Section 5 concludes the paper.

2. Model description

The OGCM used in this study is the OFES (OGCM for the Earth Simulator, [3]) which is based on the Modular Ocean Model version 3 (MOM3) [15] developed at Geophysical Fluid Dynamics Laboratory/National Oceanic and Atmospheric Administration (GFDL/NOAA), but highly optimized for the Earth Simulator (ES) with various procedure. The computational domain is quasi-global from 75°S to 75°N excluding the Arctic Ocean with the horizontal resolution of 0.1°. The number of vertical levels is 54 and the level thickness varies from 5 m for the surface to 330 m for the bottom. The model topography is constructed using the 1/30° bathymetry dataset created by the OCCAM project at the Southampton Oceanography Centre (obtained through GFDL/NOAA). The partial cell method [16] implemented in MOM3 is applied, which helps to represent the bottom topography realistically.

A hindcast simulation from July 20, 1999 to the end of 2004 (QSCAT run) is driven by daily mean surface wind stress observed by the QSCAT satellite in J-OFURO dataset [17]. The wind stress data with horizontal resolution of 1° is constructed by weighted mean method [18]. The initial oceanic field in the QSCAT run is the simulation output on July 20, 1999 from a hindcast simulation forced by daily mean NCEP/NCAR reanalysis data [5] from 1950 to 2004 (NCEP run: see Sasaki et al. [4], for details), which represents oceanic variabilities with intraseasonal-to-decadal time scales realistically. The model settings of both the QSCAT and NCEP runs are the same except the surface wind stress. The surface heat flux is calculated using the same bulk formula as in Rosati and Miyakoda [19]. The salinity flux is obtained from fresh water flux derived from the precipitation of the same reanalysis data and the evaporation estimated using the bulk formulas. In addition to the salinity flux, the surface salinity is restored to the climatological monthly mean value of the WOA98 to include the contribution from the sea-ice and river run-off. In the buffer zones within 3° latitudinal distances near the northern and southern artificial boundaries, the temperature and salinity fields are restored to the monthly mean climatological values of the WOA98 at all depths. The restoring timescale at those boundaries is set to be 1 day and it increases linearly to 720 days at 3° from the boundaries. A biharmonic operator is used for horizontal mixing of momentum and tracers to suppress computational noises with the horizontal scale of the grid spacing. Vertical viscosity and diffusivity are calculated using the K-profile parameterization (KPP) [20].

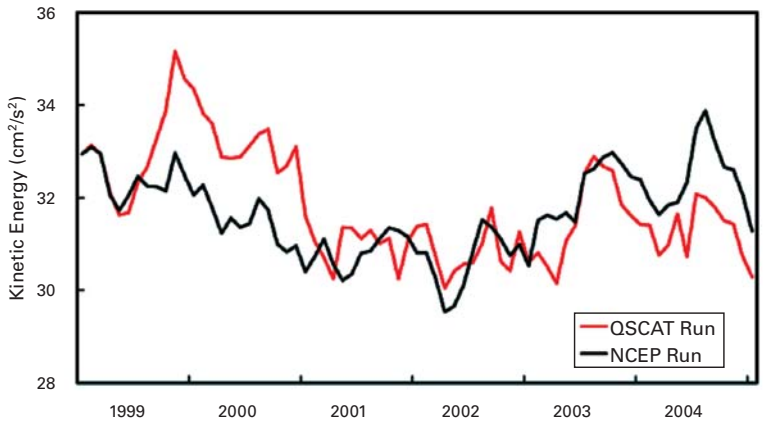

Fig. 2 Time series of global (75°S–75°N) mean kinetic energy ($cm^2\ s^{-2}$) from 1999 to 2004 based on the (red curve) QSCAT and (black curve) NCEP runs.

In the QSCAT run, it is difficult to avoid any influences from the initial condition, because of the short simulation period. In order to check the influence, the time series of the global mean kinetic energy are plotted in Figure 2. The kinetic energy in the QSCAT run increase in the latter half of 1999 and decrease in the whole year of 2000 unnaturally. In contrast to it, since 2001 the variation of the kinetic energy in the QSCAT run is comparable to that in the NCEP run. Although we suppose that the spin-up of the global oceanic field in the QSCAT run is not enough, the upper and subsurface fields may respond to the QSCAT wind stress field sufficiently after 2001. In the following analyses, we use the simulated fields after January 2001 to exclude influences of the initial shock.

The marine ecosystem model coupled with the OFES is a simple four component (NPZD) pelagic model [21]. The evolution of biological tracers is governed by an advective-diffusive equation with the source and sink terms. The source and sink terms are biological activities. The marine ecosystem model is incorporated into the both of the QSCAT and NCEP runs with the initial conditions of marine ecosystem from the 5-year biological simulation forced by the NCEP/NCAR climatological values.

3. Oceanic physical fields

The global oceanic field in the upper layer in the QSCAT run is simulated well, mostly the same as that in the NCEP run. The wind stress fields observed by the QSCAT satellite that drives the OFES makes some improvements of the representation of the oceanic fields in some regions, responding to the wind stress with small structures. The global aspects and some specific phenomenon in oceanic physical fields are reported in this section comparing with the NCEP run and observations.

3.1 Global oceanic fields

Figure 3 shows the distributions of mean surface current speed averaged from 2001 to 2004 based on the QSCAT and NCEP runs. Major currents, such as narrow strong western boundary currents and the Antarctic Circumpolar Current, are well represented in the two runs, as reported by Masumoto et al. [3] and Sasaki et al. [4]. In contrast to it, there are some differences in some regions between surface currents in the two runs, where differences between wind stress fields of the QSCAT satellite observation and NCEP/NCAR reanalysis are found (Figure 1). The distributions of the current speed in the equatorial Pacific and Atlantic and under the jets over the Central America in the eastern Pacific are much different in the QSCAT run from those in the NCEP run: in the QSCAT run, there are two zonal band-like structures along the equator in the Pacific and Atlantic associated with equatorial currents and three strip structures extending west-southwestward from the east coast of the Central America, but these are not found clearly in the NCEP run. In the west of the Hawaiian Islands, a zonal band-like structure related to the HLCC is captured in the QSCAT run, but weak in the NCEP run. In addition to it, relatively strong current speed distributions are found along the west coast of the continents in the QSCAT run, which might be associated with costal currents and coastal upwelling, consistent with the cooler SST in the QSCAT run compared with the NCEP run (not shown). These differences between the surface circulations in the two runs may be mostly attributed to the differences in small scale structures in the wind stress fields. Some specific oceanic fields in some region are depicted in Sec 3.2, and some influences in the biological fields are reported in Sec. 4.

The high-resolution in the OFES can provide us realistic eddy activities as reported in Masumoto et al. [3] and Sasaki et al. [4]. Figure 4 shows the distributions of vari-

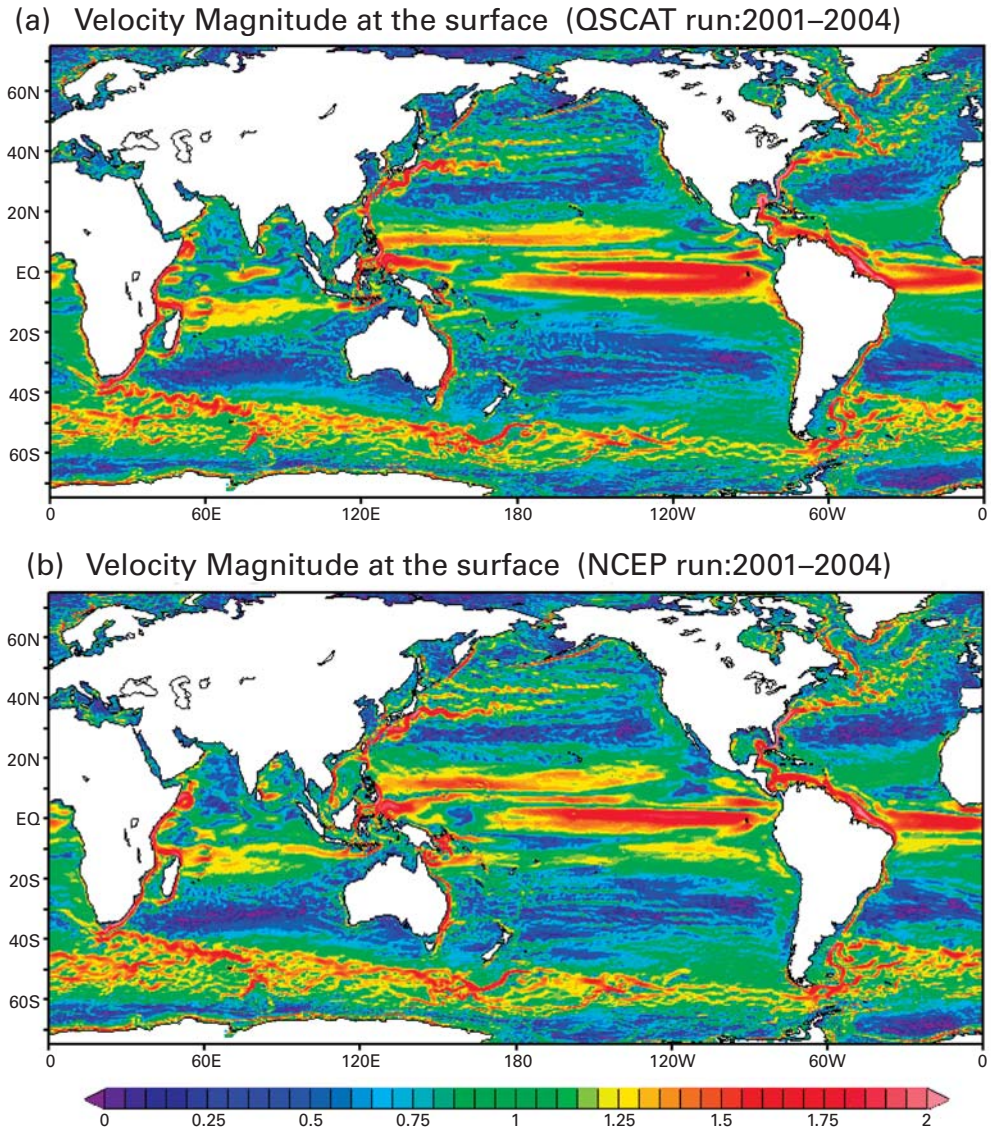

Fig. 3 Distributions of mean surface current speed in common logarithm scale (cm sec^{-1}) averaged from 2001 to 2004 based on the (a) QSCAT and (b) NCEP runs.

ability of sea surface height anomaly (SSHA) averaged from 2001 to 2004 based on the QSCAT and NCEP runs and satellite merged altimeters distributed by Aviso (Archiving, Validation, and Interpretation of Satellite Oceanographic Data project). The high variabilities along strong currents are simulated in the two runs, comparable to the satellite observation. Some improvements are found in the distribution in the QSCAT run compared to the NCEP run. In the central and eastern equatorial Pacific, SSHA variability is stronger in the QSCAT run than that in the NCEP run, and the strip structures to the west of the Costa Rica and high variability along the Panama coast are clearly found in the QSCAT run. In the western subtropical Pacific, to the west of the Hawaii Islands, two zonal band-like distributions of high variabilities are found clearly in the QSCAT run compared with the NCEP run. These improvements of the simulated variability in the QSCAT run might be related to the representations of the simulated mean currents (Figure 3) such as the equatorial currents and the subtropical countercurrents including the HLCC.

On the other hand, some discrepancies between oceanic fields of the OFES simulations and the observation, as reported in Sasaki et al. [4], are still robust even in the QSCAT run. The North Atlantic Current does not turn north and the Azores Current is not represented well. The pathway of the Agulhas Rings is too regular. Furthermore, the simulated Kuroshio has sometimes an artificial path detaching from the coasts of Kyushu Island. To overcome the problems, various model tunings such as utilizing a different kind of the parameterization in the sub-grid scale mixing processes and modification of the model bottom topography may be required.

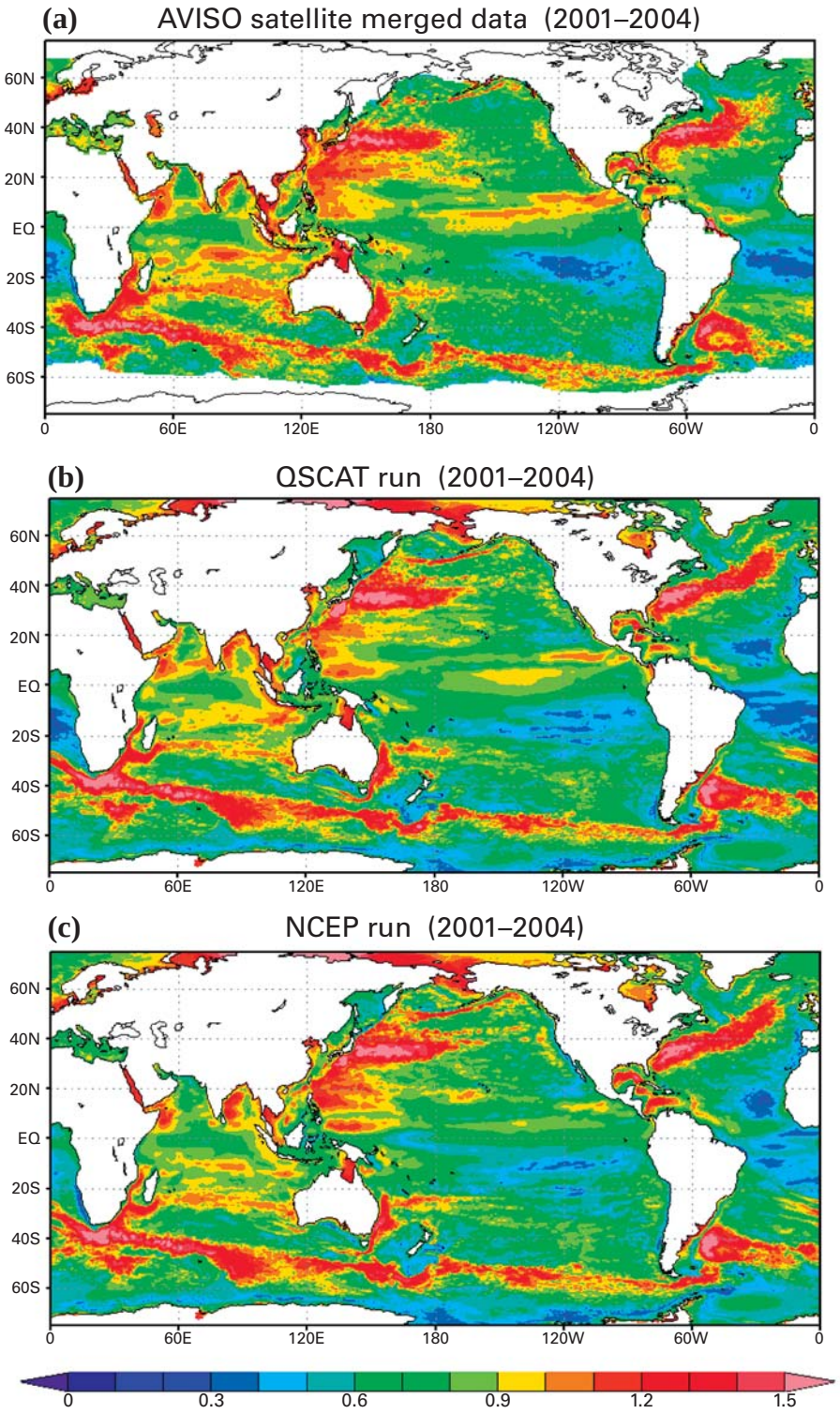

Fig. 4 Distributions of root-mean-square variances of sea surface height anomalies in common logarithm scale (cm) for 2001–2004 based on (a) the AVISO satellite observation and the (b) QSCAT and (c) NCEP runs.

3.2 Regional oceanic fields

3.2.1 Pacific equatorial currents

Masumoto et al. [3] shows that the simulated equatorial currents in the Pacific in the climatological run, forced by the monthly climatological fields of the NCEP/NCAR reanalysis, are mostly comparable to the observations. In this report, the simulated currents in the QSCAT run are compared with those in the NCEP run and the observations. Figure 5 shows meridional and longitudinal vertical sections of mean eastward current velocity averaged from

2001 to 2004 based on the QSCAT and NCEP runs. Equatorial currents including the Equatorial Undercurrent (EUC) and the other series of alternating jets: the North Equatorial Countercurrent (NECC), the Subsurface Countercurrents (SCCs), and the South Equatorial Currents (SECs) are mostly captured in the two runs compared with the observations [22, 23].

In the QSCAT run, two branches of South Equatorial

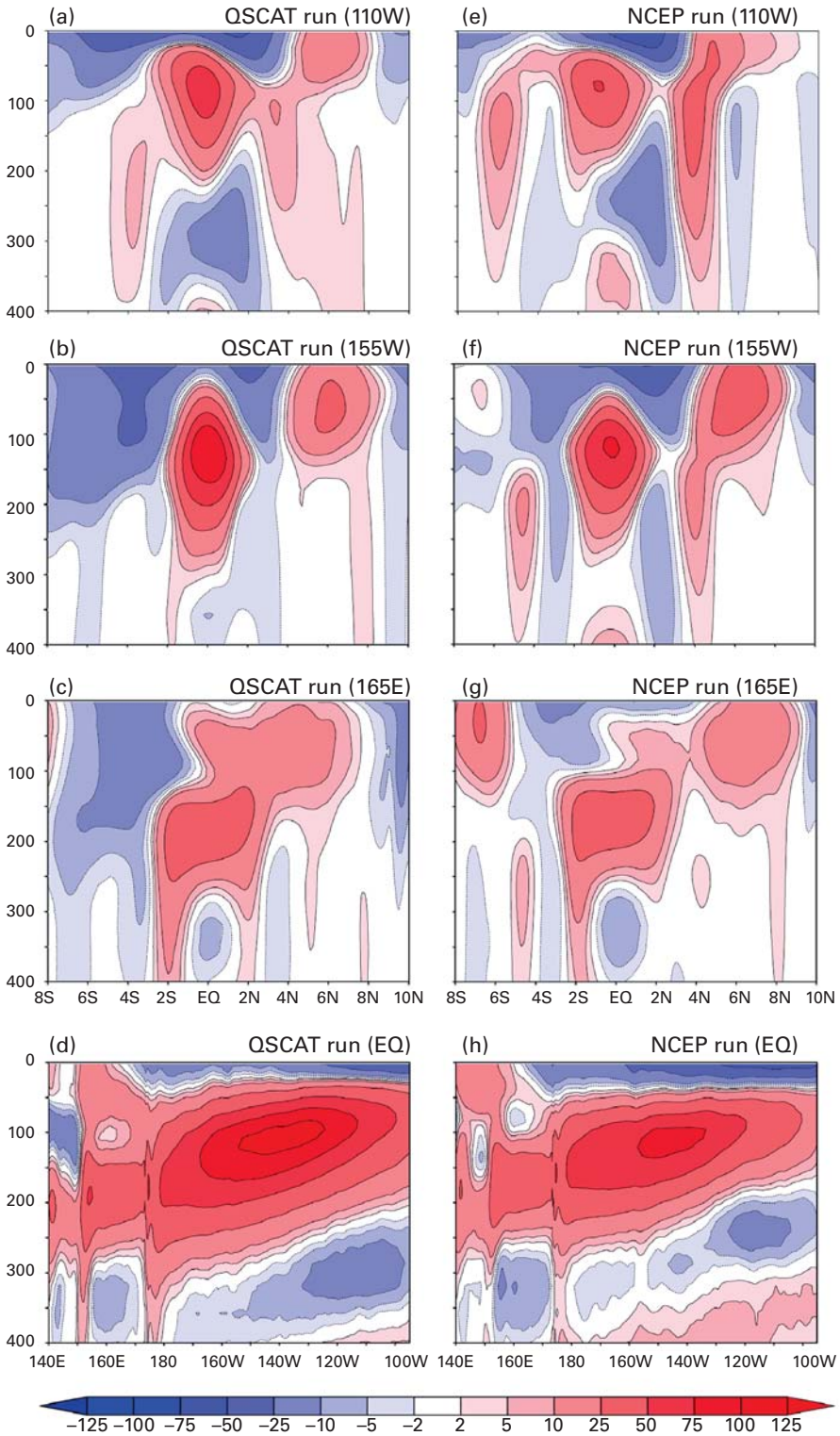

Fig. 5 Latitude-depth sections of mean eastward current speed (cm sec^{-1}) averaged from 2001 to 2004 at (a, e) 110°W, (b, f) 155°W, and (c, g) 165°E based on the (a)–(c) QSCAT and (e)–(g) NCEP runs in the equatorial Pacific. The same but longitude-depth section along the equator in the (d) QSCAT and (h) NCEP runs.

Current (SEC) are found in the upper layer at 110W° as shown in the observations: the southern and northern branches are centered at the observational latitudes of about 5°S and 2°N, respectively (Figure 5a). In the NCEP run (Figure 5e) and the climatological run (Masumoto et al. [3], their Figure 12d), however, the southern branch is not captured clearly or shifts to the south in the eastern equatorial Pacific, although the two branches are found in the central equatorial Pacific. In the QSCAT satellite wind stress fields (Figure 6a), a narrow zonal strip of positive wind stress curl is found just north of the equator in the eastern Pacific, as well as in the ERS satellite wind stress fields (not shown) as reported by Kessler et al. [23], and the zonal band of negative curl is also distributed in the south of the equator, but the both band-like structures are not found clearly in the NCEP wind stress fields (Figure 6b). It is possible that the difference between the representations of the SEC in the two runs is attributed to difference of the wind fields based on Sverdrup dynamics, although Kessler et al. [23] point out that not only Sverdrup dynamics but also the effect of the nonlinear terms through the vorticity balance play a role to drive the equatorial currents. In the equatorial Atlantic, the southern branch of the SEC is also found clearly in the QSCAT run, but obscure in the NCEP run (Figure 3). Detailed investigation of the Atlantic equatorial currents, which might be associated with the surface wind fields (Figure 1), is left for future works. Note that the QSCAT run cannot simulate well the distribution of zonal current in the subsurface in the eastern equatorial Pacific compared with that in the NCEP run, probably due to the short integration period driven by the QSCAT wind stress.

Figure 5d and 5h show that the maximum of the eastward EUC in the QSCAT run is larger than that in the NCEP run, and the eastward current speed is stronger than 1 m s^{-1} from 150°W to 125°W, consistent with the observation [22]. Relatively strong trade wind in the QSCAT wind fields (not shown) may cause strong zonal pressure gradient along the equator, and then make the EUC stronger in the QSCAT run than that in the NCEP run.

3.2.2 Hawaiian Lee Countercurrent

The Hawaiian Lee Countercurrent (HLCC) is one of narrow eastward subtropical countercurrents in the western Pacific, extending far to the west of the Hawaiian Islands [7, 24]. The QSCAT run can reproduce the west-southwestward far-reaching extent of the HLCC (Figure 7, and see closeup view in Araki et al. [25], their Figure 15 in this issue), but not in the NCEP run (not shown). The comparison between the simulated HLCCs in the QSCAT and NCEP runs is discussed in detail by Sasaki and Nonaka [26], suggesting that there are possible two-way air-sea interactions accompanying the HLCC: zonal band-like structures of wind stress curls induced by the warm HLCC in turn play a role to drive further the HLCC following the atmosphere-to-ocean and ocean-to-atmosphere feedbacks triggered by the Hawaiian Islands suggested by Xie et al. [7]. Furthermore interannual variability is suggested in both the wind field and the simulated HLCC [26]. Relatively distinct pathway of the simulated

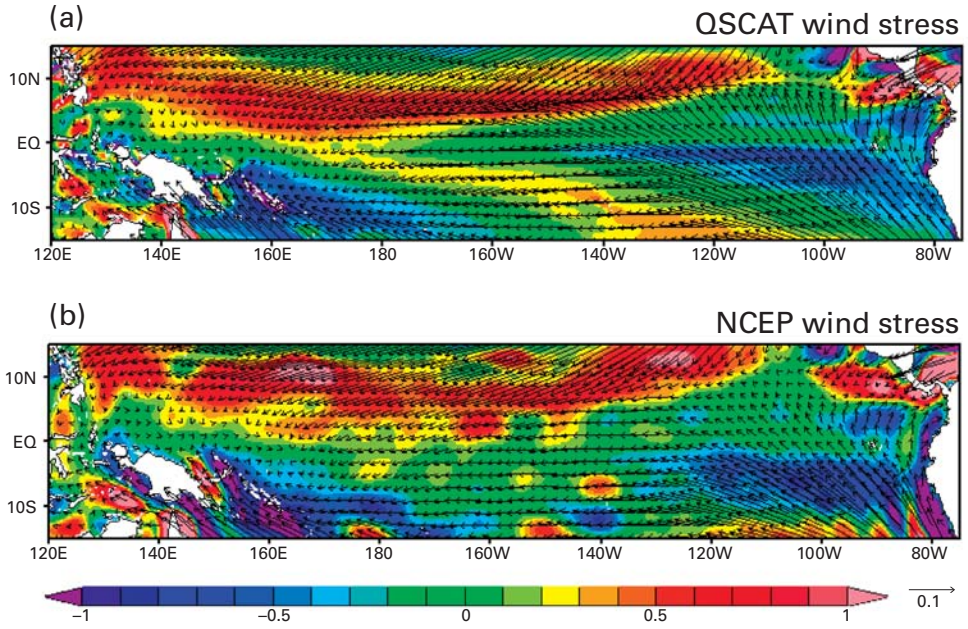

Fig. 6 Distributions of mean wind stress curl in common logarithm scale (color, unit: 10^{-7} N m^{-3}) and vectors (N m^{-2}) averaged from 2001 to 2004 in the equatorial Pacific in (a) the QSCAT satellite observation and (b) the NCEP/NCAR reanalysis.

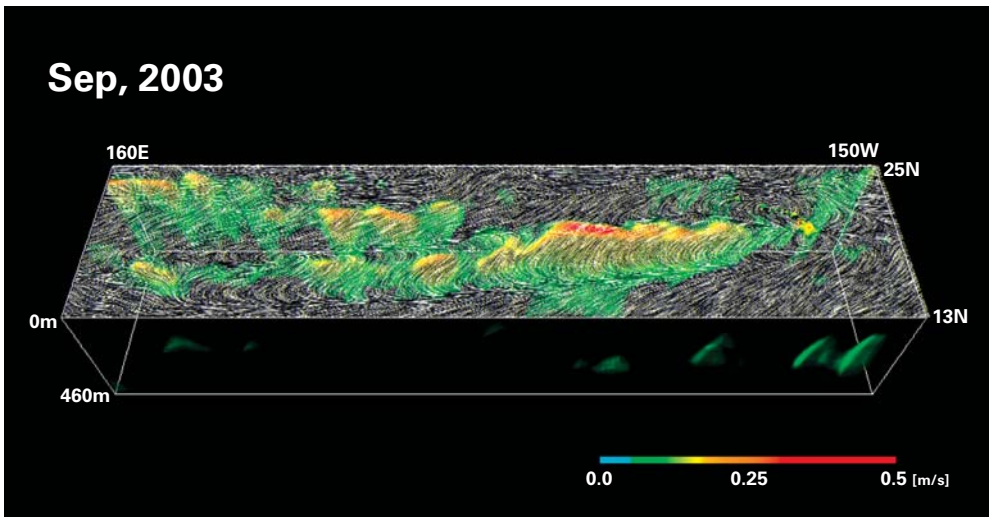

Fig. 7 3-D view of monthly mean eastward velocity (color, m sec^{-1}) and direction of high-pass filtered surface wind stress in September 2003 based on the QSCAT run. The meridional high-pass filtering is done by extracting 8° moving averages from the original data in the meridional direction, following Xie et al. [2001].

HLCC and strong elongated contrast of wind stress curls are found especially in 2003 compared with those in other years (not shown). The variability is also supported by the sea surface height fields based on the satellite observation as shown by Sasaki and Nonaka [26].

3.2.3 Loop Current Ring

It is well known that in the Gulf of Mexico the Loop Current sheds rings at irregular intervals, the periods from 3 to 17 months based on the 26-year observations [27]. The relatively large SSHA variability in the Gulf of Mexico is found in the OFES simulations and the satellite observations (Figure 4), associated with the shedding. The variability in the QSCAT run is weak compared with that in the NCEP run. A snapshot on December 31, 2004 in the NCEP run shows that the simulated Loop Current Rings pinch off realistically, however, the ring is located stationary to the north of the Yucatan Channel in the QSCAT run (Figure 8).

We discuss here the on-off status of shedding of the Loop Current Rings in the OFES simulations. Anti-cyclonic eddies are activated to the south of Hispaniola Island, and intrude into the Yucatan Channel in the NCEP run, for example eddies at 75°W and 70°W, 15°N in Figure 8b, but in the QSCAT run activities of the eddies are weak. The anti-cyclonic eddies are induced by the strong negative curl to the south of Hispaniola Island in the reanalysis, but that is weak in the satellite wind stress (Figure 1). In the NCEP run, shedding period dominates from 10 to 14 months (29 out of a total of 46 rings), and in a numerical experiment conducted by Oey et al. [28], the Loop Ring shedding in this frequency band is associated with the anti-cyclonic eddies essentially forced by mean negative wind-stress curl to the south of Hispaniola Island.

In Figure 9, the time series of the volume transport through the Yucatan Channel are plotted based on the two runs and the climatological run [3]. The transports averaged from 2001 to 2004 are 17.1 Sv (1 Sv = 1.0×10^6 m^3 sec^{-1}) in the QSCAT run, and 20.2 Sv in the NCEP run, respectively. The transport in the QSCAT run is much less than 23.6 Sv in the observation [29], and suddenly decreases between the end of 2001 and the beginning of 2002, at the same time the rings stop being shed. In the Atlantic Ocean, the volume transport of western boundary current estimated from the QSCAT satellite wind stress based on the Sverdrup theory is comparable to that estimated from the NCEP/NCAR reanalysis (not shown). Thus, the decreasing in the transport in the QSCAT run might be attributed to the differences between the local wind stress fields in the Caribbean Sea in the satellite observation and the reanalysis, although its mechanism is unclear. This is consistent with a model experiment study by Oey et al. [28], which shows that the strength of mean transport through the Yucatan Channel depends largely on wind stress field in the Caribbean Sea. Note that the transport through the Yucatan Channel in the QSCAT run after the decreasing is comparable to that in the climatological run, in which the ring is located stationary (not shown). The time-dependent variation in the wind might also be one of key factors to simulate the ring shedding, as implied by Oey et al. [28]. Thus, these comparisons suggest that in the case of OFES simulations the on-off status of the Loop Current Ring shedding may be associated with the strength of mean transport, and activities of

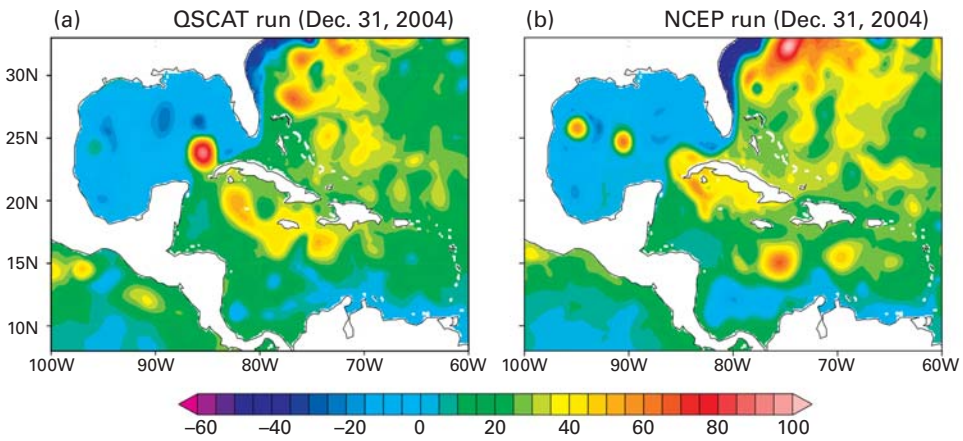

Fig. 8 Snapshots of sea surface height (cm) in the Gulf of Mexico on December 31, 2004 in the (a) QSCAT and (b) NCEP runs.

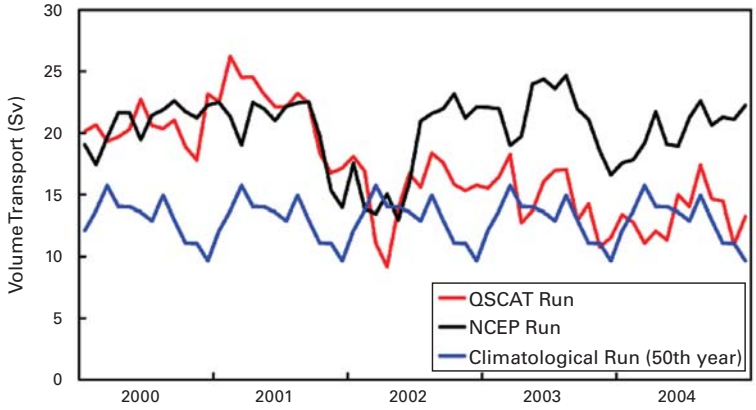

Fig. 9 Time series of volume transport (Sv: 10^6 m^3 sec^{-1}) through the Yucatan Channel based on the (red curve) QSCAT and (black curve) NCEP runs from 2000 to 2004. The transport based on (blue curve) the climatological run in the model 50th year is plotted cyclically.

anticyclonic eddies induced by the wind stress field. Additionally, a distinct pattern of the wind stress curl is found in the Loop Current region based on the QSCAT satellite observation, suggesting possible feedback of the current on the wind-stress field [30]. Therefore, further detailed analyses including consideration of a local air-sea interaction are necessary to understand how the changes in the transport are induced and how the transport changes relate to the shedding of the ring. At the same time, longer integration of the QSCAT run is necessary to compare statistical properties of the rings with the counterparts in the NCEP run.

4. Oceanic biological fields

The NCEP and QSCAT runs simulate biological fields with a four component NPZD ecosystem model. We introduce here the surface distributions of chlorophyll in the North Pacific and along the California coast comparing the two runs and the observation.

4.1 North Pacific

Seasonal variability of surface chlorophyll concentration is shown in Figure 10 and 11 compared with the MODIS (Moderate Resolution Imaging Spectroradiometer) satellite images. Qualitatively, the model reproduces well the chlorophyll distribution pattern, particularly in the upwelling region off California and the Kuroshio and Kuroshio Extension regions. With the eddy-resolving horizontal resolutions, the OFES can capture a realistic mesoscale phenomena (eddy, front, and upwelling) and western boundary currents [3]. In spring, however, simulated chlorophyll concentrations (0.8 – 1.0 mg m^{-3}) are larger than the MODIS image (0.2 – 0.4 mg m^{-3}) except coastal regions and marginal seas (Figure 10). In the coastal regions and marginal seas, simulated chlorophyll concentrations (< 2.0 mg m^{-3}) are lower than the MODIS image (> 5.0 mg m^{-3}). In fall, the model shows a good qualitative agreement with the pattern of the MODIS image, but simulated chlorophyll concentrations (< 1.0 mg m^{-3}) are lower

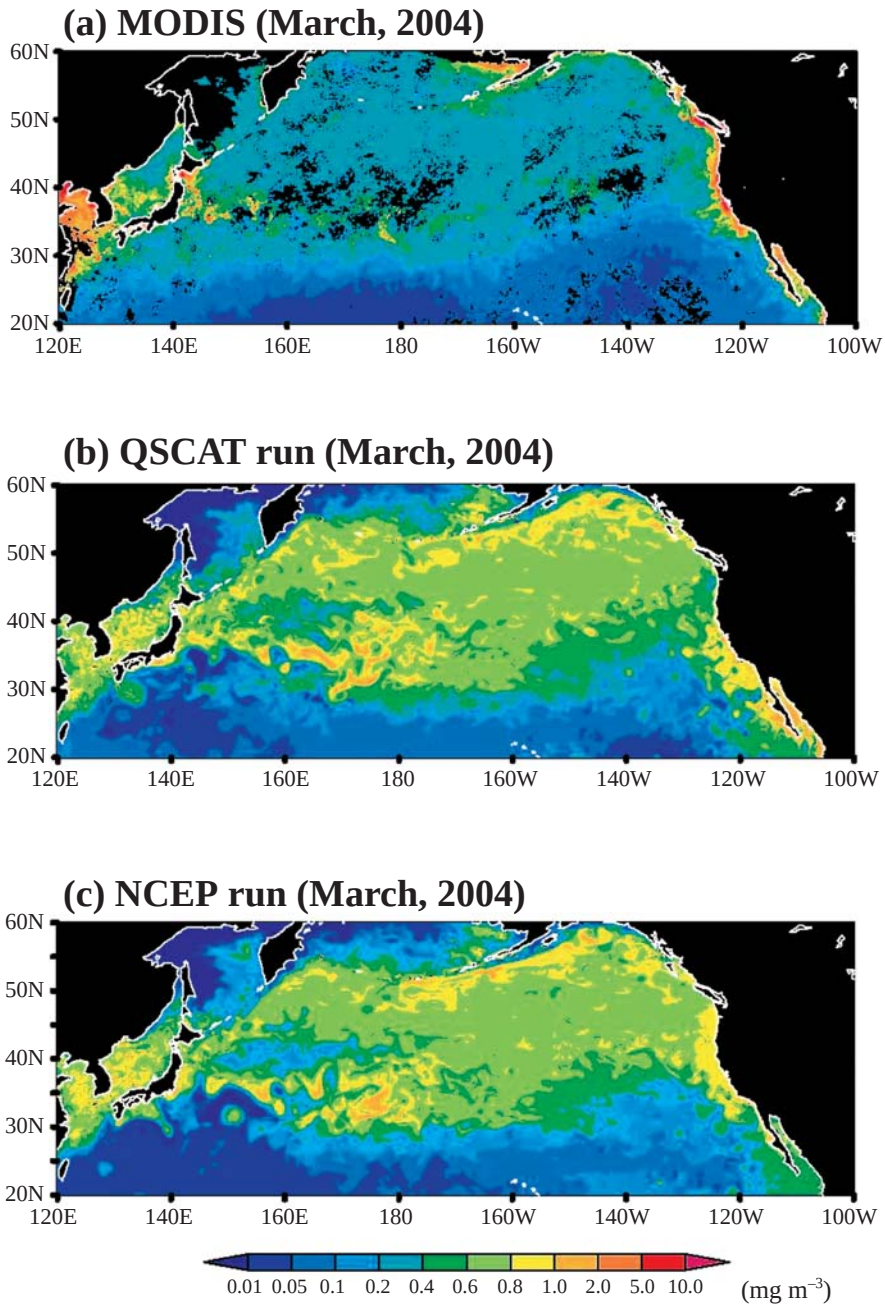

Fig. 10 Distribution of surface chlorophyll concentration (mg m^{-3}) in March: (a) MODIS satellite image, (b) QSCAT run, and (c) NCEP run.

than the MODIS image, especially in the coastal regions and the Bering Sea and the Gulf of Alaska (Figure 11).

Photosynthesis in the model is a function of light intensity, temperature, and nitrate concentration. In spring, simulated chlorophyll concentrations are overestimated in the subpolar regions (Figure 10). The biological model may not sufficiently represent the timing of spring bloom and phytoplankton growth rate. In fall, simulated chlorophyll concentrations in the coastal regions are underestimated (Figure 11). Since the model does not include nutrient input from rivers, in the Bering Sea, the Gulf of Alaska, and marginal seas, the simulated chlorophyll concentrations are lower than that in the satellite image.

Large difference of surface chlorophyll pattern between the NCEP and QSCAT runs is found in the eastern boundary. Because wind field is important factor for driving the eastern boundary current and coastal upwelling, small-scale features of the QSCAT wind field affect the eastern boundary current system. The pattern of the surface chlorophyll distribution in the QSCAT run is close to that of the MODIS image, compared with the NCEP run. Then, as an example, detailed structure in the region along the California coast is investigated in the next section.

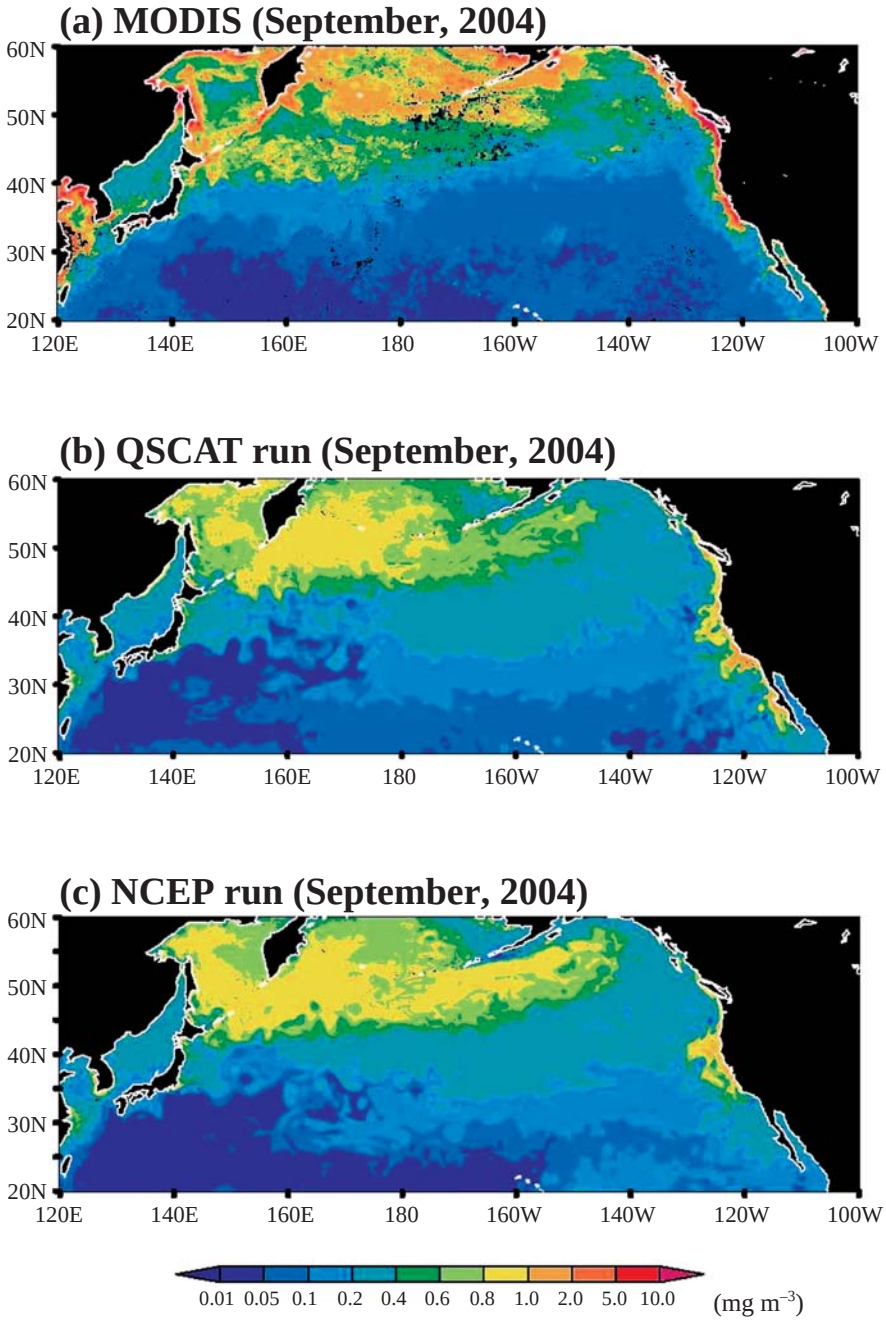

Fig. 11 Distribution of surface chlorophyll concentration (mg m^{-3}) in September: (a) MODIS satellite image, (b) QSCAT run, and (c) NCEP run.

4.2 California Coast

The direction of wind along the California coast changes according to seasons: southerly winds in winter and northerly winds in summer. Figure 12 shows the physical and biological fields along the California coast in the strong northerly wind season (September). SST near the coast in the QSCAT run (< 12°C; Figure 12a) is lower than that in the NCEP run (< 14°C; Figure 12e). Small-scale variability of eastern boundary current is also shown in Figure 12a. Vertical velocity near the coast in the QSCAT run is stronger and has a smaller horizontal scale (Figure 12b) than that in the NCEP run (Figure 12f). This result shows that the near-shore wind field has a strong influence for the coastal upwelling. High nitrate water at the subsurface layer and high chlorophyll at the surface are shown near the coast in the QSCAT run (Figures 12c and 12d), but in the NCEP run, these distributions extend offshore (Figure 12g and 12h). The simulated chlorophyll pattern in the QSCAT is more similar to the MODIS satellite image than that in the NCEP run. Using the QSCAT wind field in the eddy-resolving ocean model, it is possible to improve the biological field in the

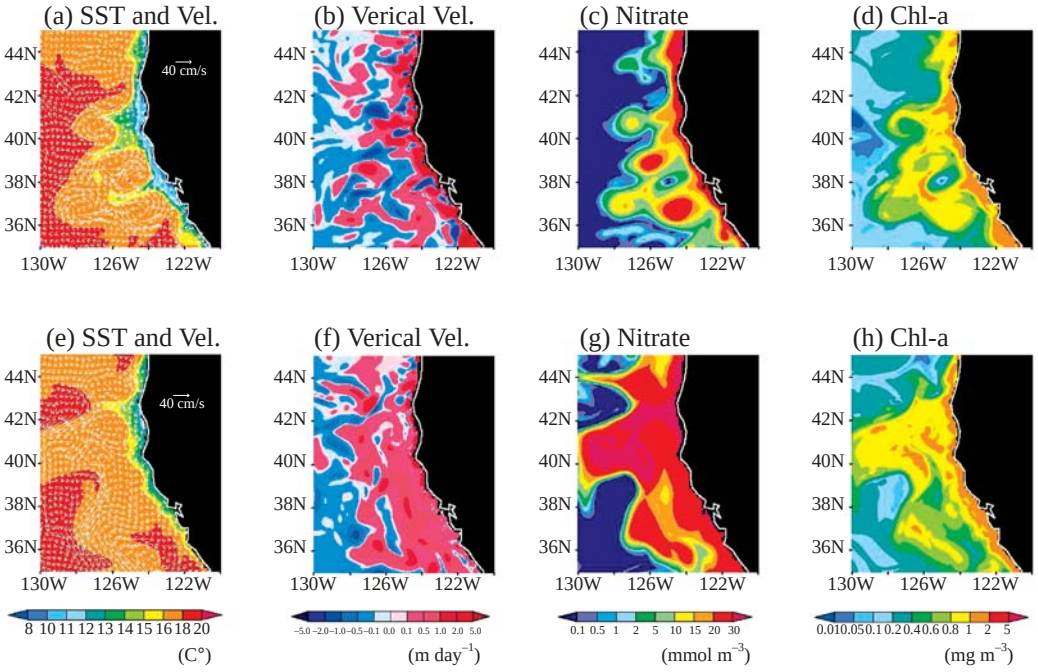

Fig. 12 Distributions of (a, e) sea surface temperature (°C) with the current vectors (cm s^{-1}), at 25 m depth, (b, f) vertical velocity (m day^{-1}) at 60 m depth, (c, g) nitrate concentration (mmol m^{-3}) at 60 m depth, and (d, h) surface chlorophyll concentration (mg m^{-3}) in the California coast in September: (a)–(d) QSCAT run and (e)–(h) NCEP run.

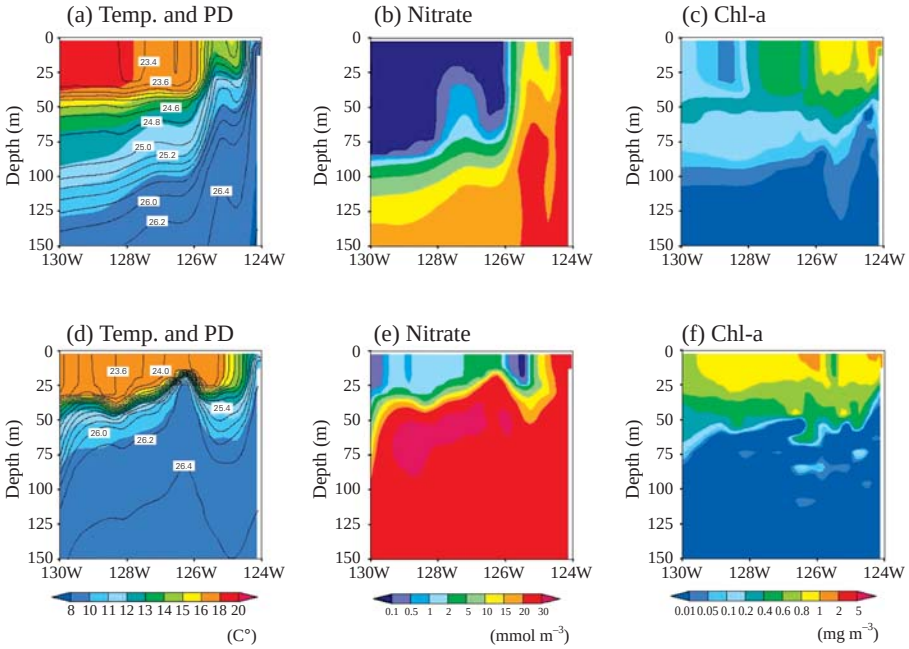

Fig. 13 Vertical distribution of (a, d) temperature (°C) with the potential density, (b, e) nitrate concentration (mmol m^{-3}), and (c, f) chlorophyll concentration (mg m^{-3}) along 40°N in September: (a)–(c) QSCAT run and (d)–(f) NCEP run.

eastern boundary coastal region.

The temperature, nitrate concentration, and chlorophyll concentration along 40°N show the different vertical distributions influenced by the different upwelling structures (Figure 13). Coastal SST in the QSCAT is 12°C colder than that in the NCEP run (Figure 13a and 13d). The slope of isopycnal layers in the QSCAT run is steeper than that in the NCEP run. Distribution of nitrate concentration is mainly influenced by the physical environment. Offshore nitrate concentration (< 0.1 mmol m^{-3}) in the

QSCAT run is much lower than that (< 5 mmol m^{-3}) in the NCEP run (Figure 13b and 13e). The bloom (0.8 – 1 mg m^{-3}) in the QSCAT run occurs near the coast, but the occurrence of bloom (0.8 – 1 mg m^{-3}) in the NCEP run extends offshore (Figure 13c and 13f).

5. Conclusions

The OFES simulation driven by the realistic wind stress field observed by the QSCAT satellite has been performed on the ES. The simulated oceanic fields are improved in some regions in comparison with those driven by the NCEP reanalysis wind stress, as the fields represent well responses to small scale structures in the satellite wind field associated with orographic effects, air-sea interactions, and coastlines. In the QSCAT run, the far-reaching HLCC extends west-southwestward in the lee of the Hawaiian Islands realistically, and the equatorial current system including two branches of the SEC is represented well in association with zonal band-like structures of the wind curls. Realistic representation of the responses to the small scale structures in the satellite wind fields are extended to the simulated biological fields in the regions influenced by the near-shore wind field, for example along the California coast. In addition, the on-off status of the Loop Current Ring shedding in the OFES simulations is discussed in this paper, which seems to be related to the mean volume transport through the Yucatan Channel and eddy activity in the Caribbean Sea induced by local wind stress field.

Although the enormous power of contemporary super computer systems such as the ES enables us to perform eddy-resolving global ocean simulations in the practical time, even now it is still not easy to perform lots of the sensitivity experiments due to limited computational resource and storage system. The comparison between the simulations driven by two different wind stress fields in this study provides one example of such sensitivity experiments, suggesting that high resolutions of spatial scales in the forcing data may be one of key factors to succeed realistic representations in the simulated oceanic fields with small-scale features. Some of our future simulations using the OFES will be driven by wind stress with higher horizontal resolution, for example 0.5° or 0.25°, which are expected to provide more insights of responses of oceanic fields to the wind stress with smaller scale structures in eddy-resolving simulations.

Acknowledgments

We are grateful to OFES project members including Drs. H. Sakuma and A. Ishida and researchers in Atmosphere and Ocean Simulation Research Group in The Earth Simulator Center. Our thanks are extended to Drs. S.-P. Xie and F. Araki for valuable discussions and advanced visualizations respectively. QuikSCAT wind stress data in the J-OFURO dataset (http://dtsv.scc.u-tokai.ac.jp/j-ofuro/) are provided by Dr. K. Kutsuwada. Dynamic SSH data and the satellite images were obtained from AVISO (http://www.aviso.oceanobs.com) and MODIS (http://oceancolor.gsfc.nasa.gov/), respectively. The OFES simulations were conducted on the Earth Simulator under support of JAMSTEC.

(This article is reviewed by Dr. Julia Slingo.)

References

[1] M. E. Maltrud and J. L. McClean, An eddy resolving global 1/10° ocean simulation, *Ocean Modelling*, vol.**8**, pp.31–54, 2005.

[2] D. J. Webb, Evidence for shallow zonal jets in the South Equatorial Current region of the Southwest Pacific, *J. Phys. Oceanogr.*, vol.**30**, pp.706–720, 2000.

[3] Y. Masumoto, H. Sasaki, T. Kagimoto, N. Komori, A. Ishida, Y. Sasai, T. Miyama, T. Motoi, H. Mitsudera, K. Takahashi, H. Sakuma, and T. Yamagata, A fifty-year eddy-resolving simulation of the world ocean: Preliminary outcomes of OFES (OGCM for the Earth Simulator), *J. Earth Sim.*, vol.**1**, pp.35–56, 2004.

[4] H. Sasaki, M. Nonaka, Y. Masumoto, Y. Sasai, H. Uehara, and H. Sakuma, An eddy-resolving hindcast simulation of the quasi-global ocean from 1950 to 2003 on the Earth Simulator, in *High resolution numerical modelling of the atmosphere and ocean*, edited by K. Hamilton and W. Ohfuchi, Springer, New York, in press.

[5] E. Kalnay, M. Kanamitsu, R. Kistler, W. Collins, D. Deaven, L. Gandin, M. Iredell, S. Saha, G. White, J. Woollen, Y. Zhu, M. Chelliah, W. Ebisuzaki, W. Higgins, J. Janowiak, K.C. Mo, C. Ropelewski, A. Leetmaa, R. Reynolds, and R. Jenne, The NCEP/NCAR 40-year reanalysis project, *Bull. Amer. Meteor. Soc.*, vol.**77**, pp.437–471, 1996.

[6] W. T. Liu, X. Xie, P. S. Polito, and S.-P. Xie, Atmospheric manifestation of tropical instability wave observed by QuikSCAT and Tropical Rain Measuring Mission, *Geophys. Res. Lett.*, vol.**27**, pp.2545–2548, 2000.

[7] S.-P. Xie, W. T. Liu, Q. Liu, and M. Nonaka, Far-reaching effects of the Hawaiian Islands on the Pacific ocean-atmosphere system, *Science*, vol.**292**, pp.2057–2060, 2001.

[8] D. B. Chelton, S. K. Esbensen, M. G. Schlax, N. Thum, M. H. Freilich, F. J. Wentz, C. L. Gentemann, M. J. McPhaden, and P. S. Schopf, Observations of coupling between surface wind and seasurface temperature in the eastern tropical Pacific, *J. Clim.*, vol.**14**, pp.1479–1498, 2001.

[9] S.-P. Xie, H. Xu, W. S. Kessler, and M. Nonaka, Air-sea

interaction over the eastern Pacific warm pool; gap winds, thermocline dome, and atmospheric convection, *J. Clim.*, vol.**18**, pp.5–20, 2005.

[10] A. Oschlies and V. Garçon, An eddy-permitting coupled physical-biological model of the North Atlantic: 1. Sensitivity to advection muerics and mixed layer physics, *Glob. Biogeochem. Cycles*, vol.**13**, pp.135–160, 1999.

[11] A. Oschlies, W. Koeve, and V. Garçon, An eddy-permitting coupled physical-biological model of the North Atlantic: 2. Ecosystem dynamics and comparison with satellite and JGOFS local station data, *Glob. Biogeochem. Cycles*, vol.**14**, pp.499–523, 2000.

[12] A. Oschlies, Can eddies make ocean deserts bloom?, *Glob. Biogeochem. Cycles*, vol.**16**, 1106, doi:10.1029/ 2001 GB001830, 2002.

[13] Y. Sasai, A. Ishida, H. Sasaki, S. Kawahara, H. Uehara, and Y. Yamanaka, A global eddy-resolving coupled physical-biological model: Physical influences on a marine ecosystem in the North Pacific, in *Open International Conference on Modeling and Simulation - OICMS 2005*, edited by D.R.C. Hill, V. Barra, and M.K. Troer, Blaise Pascal University, France, pp.129–138, 2005.

[14] X. J. Capet, P. Marchesiello, and J. C. McWilliams, Upwelling response to coastal wind profiles, *Geophys. Res. Lett.*, vol.**31**, L13311, doi:10.1029/2004GL020123, 2004.

[15] R. C. Pacanowski and S. M. Griffies, The MOM 3 Manual, *GFDL Ocean Group Technical Report* No.4, Princeton, NJ: NOAA/Geophysical Fluid Dynamics Laboratory, 680pp, 1999.

[16] R. C. Pacanowski and A. Gnanadesikan, Transit response in a z-level ocean model that resolves topography with partial-cells, *Mon. Wea. Rev.*, vol.**126**, pp.3248–3270, 1998.

[17] M. Kubota, N. Iwasaka, S. Kizu, M. Konda, and K. Kutsuwada, Japanese ocean flux data sets with use of remote sensing observations (J-OFURO), *J. Oceanogr.*, vol.**58**, pp.213–225, 2002.

[18] K. Kutsuwada, Impact of wind/wind-stress field in the North Pacific constructed by ADEOS/ NSCAT data, *J. Oceanogr.*, vol.**54**, pp.443–456, 1998.

[19] A. Rosati and K. Miyakoda, A general circulation model for upper ocean circulation, *J. Phys. Oceanogr.*, vol.**18**, pp.1601–1626, 1988.

[20] W. G. Large, J.C. McWilliams, and S.C. Doney, Oceanic vertical mixing –a review and a model with a nonlocal boundary layer parameterization, *Rev. Geophys.*, vol.**32**, pp.363–403, 1994.

[21] A. Oschlies, Model-derived estimates of new production: New results point towards lower values, *Deep-Sea Res.*, vol.**48**, pp.2173–2197, 2001.

[22] G. C. Johnson, B. M. Sloyan, W. S. Kessler, and K. E. McTaggart, Direct measurements of upper ocean currents and water properties across the tropical Pacific Ocean during the 1990's, *Prog. Oceanogr.*, vol.**52**, pp.31–61, 2002.

[23] W. S. Kessler, G. C. Johnson, and D. W. Moore, Sverdrup and nonlinear dynamics of the Pacific Equatorial Currents, *J. Physics. Oceanogr.*, vol.**33**, pp.994–1008, 2003.

[24] P. Flament, S. Kennan, R. Lumpkin, M. Sawyer, and E. Stroup, The ocean, in *Atlas of Hawaii*, edited by S. P. Juvik and J. O. Juvik, Univ. of Hawaii Press, Honolulu, pp.82–86, 1998.

[25] F. Araki, H. Uehara, N. Ohno, S. Kawahara, M. Furuichi, and A. Kageyama, Visualization of large-scale data generated by Earth Simulator, *J. Earth Sim.*, vol.**6**, pp.25–34, 2006.

[26] H. Sasaki and M. Nonaka, Far-reaching Hawaiian Lee Countercurrent driven by wind-stress curl induced by warm SST band along the current, *Geophys. Res. Lett.*, vol.**33**, L13602, doi:10.1029/2006GL026540, 2006.

[27] W. Sturges and R. Leben, Frequency of ring separations from the Loop Current in the Gulf of Mexico: a revised estimate, *J. Physic. Oceanogr.*, vol.**30**, pp.1814–1819, 2000.

[28] L.-Y. Oey, H.-C. Lee, and W. J. Schmitz Jr., Effects of winds and Caribbean eddies on the frequency of Loop Current eddy shedding: a numerical study, *J. Geophys. Res.*, vol.**108**, 3324, doi:10.1029/2002JC001698, 2003.

[29] J. Sheinbaum, J. Candela, A. Badan, and J. Ochoa, Flow structure and transport in the Yucatan Channel, *Geophys. Res. Lett.*, vol.**29**, doi:10.1029/2001GL013990, 2002.

[30] D. B. Chelton, M. G. Schlax, M. H. Freilich, and R. F. Milliff, Satellite measurements reveal persistent small-scale features in ocean winds, *Science*, vol.**303**, pp.978–983, 2004.